Computing one-dimensional metasurfaces

J. B. Pendry, Paloma A. Huidobro, and Kun Ding
The Blackett Laboratory, Department of Physics, Imperial College London, London SW7 2AZ, United Kingdom

(Received 23 September 2018; revised manuscript received 2 January 2019; published 7 February 2019)

We show that complex periodic metasurfaces can be simply represented by conformal transformations from the flat surface of a slab of material to a periodic grating leading to a methodology for computing their properties. Matrix equations are solved to give accurate solutions of Maxwell's equations with detailed derivations given in the Supplemental Material.

DOI: 10.1103/PhysRevB.99.085408

I. INTRODUCTION

In this paper we propose a methodology accurate at the level of Maxwell's equations for analyzing one-dimensional (1D) structures imprinted upon a 2D surface.

Transformation optics is a powerful tool used to analyze complex structures. It exploits the invariant form of Maxwell's equations under coordinate transformations: only the values of ε, μ change under a transformation. This property has been exploited to simplify computer codes [1] and to design cloaks [2–4]. A review can be had in Ref. [5]. Conformal transformations in 2D are a special case as they leave ε, μ unchanged in the 2D plane and have been long exploited to solve problems in electrostatics [6]. In the past we and others have used conformal transformations to analyze subwavelength plasmonic systems where a quasistatic approximation is accurate [7–10]. Retardation can be added as a perturbation to give an accurate account of their optical properties and at the same time the transformations reveal startling relationships between the transformed systems. However, where surfaces and metasurfaces are concerned retardation is not a perturbation and we must find solutions to the full set of Maxwell's equations [11]. Also it is useful to be able to calculate the out-of-plane response of a metasurface where the fields are no longer confined to the 2D plane of the conformal transformation.

A related approach, also based on coordinate transformations, has been taken by Chandezon *et al.* [12] and by Barnes *et al.* [13]. Our method differs in being based on conformal transformations and although the numerics are rather similar, conformal transformations have the advantage of giving more physical insight: for example, by revealing hidden properties of the metasurface such as the otherwise unexpected degeneracy of dispersion curves as we shall describe later in the paper.

Metamaterials are materials structured on a scale less than the wavelength and much attention has been concentrated on metasurfaces where the structure is confined to the surface region, and a wealth of technology enables sophisticated engineering of these structures [12–20]. In this paper we concentrate on 1D surface structures, which in essence are complex gratings but which, as we shall show, can have responses far more interesting than the simple diffraction effects shown by conventional gratings. This is particularly true when the surface in question is metallic, supporting short wavelength surface plasmons [21]. Gratings couple external radiation to surface plasmons, dramatically so when the transformations are singular [22]. At the same time the precise configuration of the surface structure changes the nature of the surface plasmons.

In our approach we assume that the metasurface is defined as an interface between two media within each of which the permittivity is constant. We exploit the observation that any single valued surface (i.e. a surface that in Fig. 1 has one value of x for every value of y) can be transformed to a flat surface by a conformal mapping between two coordinate systems,

$$z = z(w), \tag{1}$$

where z and w are complex variables,

$$z = x + iy, \quad w = u + iv. \tag{2}$$

For example a series of mappings takes a flat surface into the surface of a cylinder,

$$w' = e^{w}, \tag{3}$$

whose surface can then be distorted in an arbitrary fashion,

$$z' = z'(w'), \tag{4}$$

and finally unwrapped into a second surface with periodic structure in the v axis,

$$z = \Gamma \ln z'. \tag{5}$$

The three mappings are shown in Fig. 1. The only limitation is that the metasurface should be single valued.

Conformal mappings [23] have been utilized to solve electrostatic problems where the potential $\varphi(z)$ automatically obeys the 2D Laplace equation if it is an analytic function of z. Making a transformation and evaluating the potential in the new frame, $\varphi(w)$, yields a function which also obeys Laplace. Hence, solving the problem in one frame gives solutions in all transformed frames.

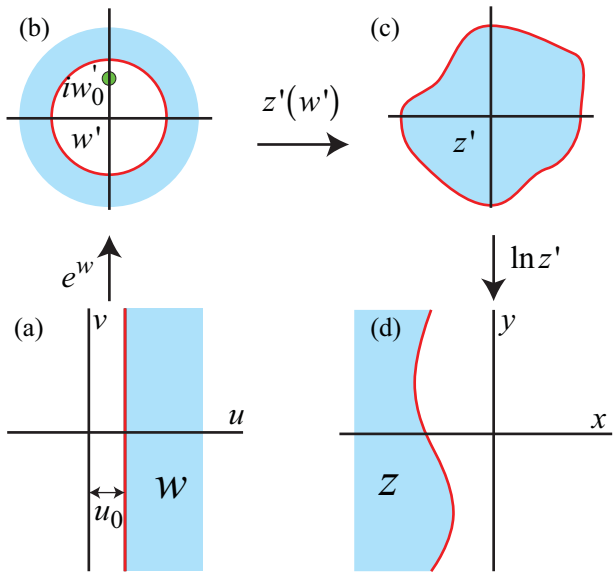

FIG. 1. A series of conformal tranformations takes a flat surface to a metasurface.

At first sight this observation leads to a paradox: if any surface can be conformally mapped to a flat surface then logic dictates that in the quasistatic limit both surfaces share the same spectrum. The flaw in this argument is that for this to be true the mappings have to be conformal *and analytic,* which in general they are not. If present, branch cuts introduced by singularities require additional sets of boundary conditions that spoil the argument [24]. However, there are some transformations for which there are no branch cuts, or where the branch cuts can be ignored.

In this paper we break free of restrictions to in-plane quasistatic solutions allowing full electromagnetic solutions of any polarization, but still exploiting other advantages of a conformal description of the metasurface. We adopt the coordinate definition given in Fig. 2 in which the surface normal is the x axis, the y axis is normal to the lines of the grating, and the s axis is parallel to the lines. The x, y coordinates can be represented by a complex number $z = x + iy$. In 1D structures the system remains translationally invariant along the s axis

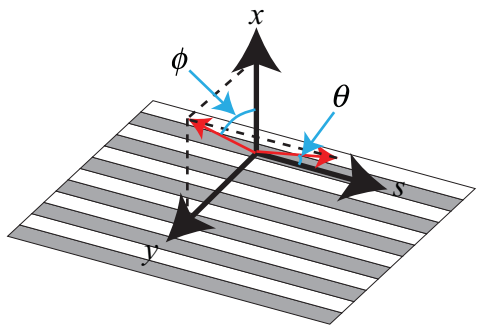

FIG. 2. Definition of the three axes, x, y, s. The angles θ, ϕ define the wave vector, with components $k_x, k + g$ and k_s, where g is the reciprocal lattice spacing [see Eq. (8)].

and all transformations used to generate the metasurface are confined to the x, y plane.

A simple rule [25] gives the values of ε, μ in the transformed frame: if we compress the x coordinates by a factor of β, then in the transformed frame components of ε, μ along this direction are reduced by a factor of β, those in the y, s directions are increased by β^{-1}. If the transformation is to be conformal, i.e., to preserve angles in the x, y plane, then there must also be a compression of β along the y axis. As a result, our formulas show that the two compressions cancel in the x, y plane but leave the s components increased by β^{-2}. This invariance of in-plane components accounts for the value of conformal transformations in 2D quasistatic problems where electric fields are confined to the x, y plane. In the general solution that follows, fields can have any orientation and do not obey Laplace, nevertheless we can exploit the invariance of ε, μ in the x, y plane to navigate our way around the boundary matching problem.

Conformal transformations are most applicable to 2D problems where there is a well-known recipe for a transformation to be conformal. To extend these ideas 3D systems, i.e., 2D metasurfaces, would require application of the full scope of transformation optics and is beyond the scope of the present paper.

II. THE FORMALISM

In the general case we must work with both electric and magnetic fields. We choose to define the two possible polarizations as S, where the magnetic fields are confined to the x, y plane, and P where the electric fields are confined to the x, y plane. The axes are defined in Fig. 2. Note that the choice of polar coordinates is not the conventional one for surfaces.

We write the incident fields in the metasurface frame,

$$\begin{aligned}\mathbf{H}^{S\,\mathrm{inc}} &= \sum_g \left(H_{gx}^{S\,\mathrm{inc}}\hat{\mathbf{x}} + H_{gy}^{S\,\mathrm{inc}}\hat{\mathbf{y}}\right)\mathrm{e}^{-ik_{gx}x+i(k+g)y+ik_s s},\\ \mathbf{E}^{P\,\mathrm{inc}} &= \sum_g \left(E_{gx}^{P\,\mathrm{inc}}\hat{\mathbf{x}} + E_{gy}^{P\,\mathrm{inc}}\hat{\mathbf{y}}\right)\mathrm{e}^{-ik_{gx}x+i(k+g)y+ik_s s},\end{aligned} \tag{6}$$

where

$$k_{gx}^2 + (k+g)^2 + k_s^2 = \varepsilon k_0^2 = \varepsilon\omega^2 c_0^{-2}, \tag{7}$$

ω is the frequency, and c_0 is the velocity of light in free space. The permittivity of the medium is given by ε. The grating spacing $a = 2\pi\ \Gamma$ defines the reciprocal lattice vectors,

$$g = n/\Gamma, \tag{8}$$

where n is an integer. The associated electric fields for S polarization, and magnetic fields for P polarization, are to be had from Maxwell's equations. In general, the metasurface will mix the two polarizations.

The unknowns to be determined are: waves leaving the surface defined by $\mathbf{H}^{S\,\mathrm{ref}}$, $\mathbf{E}^{P\,\mathrm{ref}}$; inside the medium there will, in general, be waves incident on the surface from sources within the medium, $\mathbf{H}^{S\,\mathrm{iin}}$, $\mathbf{E}^{P\,\mathrm{iin}}$, and waves leaving the surface heading deeper into the medium, $\mathbf{H}^{S\,\mathrm{trans}}$, $\mathbf{E}^{P\,\mathrm{trans}}$. We solve for these fields by requiring that field components parallel to

the surface match across the boundary. This can be done in any frame of reference but is most easily done in the w frame, where the surface is defined to be flat. Using the well-known formulas,

$$H_u^S = H_x^S \frac{\partial x}{\partial u} + H_y^S \frac{\partial y}{\partial u} = H_x^S \frac{\partial y}{\partial v} - H_y^S \frac{\partial x}{\partial v},$$
$$H_v^S = H_x^S \frac{\partial x}{\partial v} + H_y^S \frac{\partial y}{\partial v} = -H_x^S \frac{\partial y}{\partial u} + H_y^S \frac{\partial x}{\partial u}, \tag{9}$$

with similar expressions for E_u^P, E_v^P. The spatial dependence of the fields is calculated by first writing the x, y coordinates in complex notation,

$$x = \frac{1}{2}(z + z^*), \quad y = \frac{1}{2i}(z - z^*), \tag{10}$$

then substituting for z in terms of w,

$$\mathbf{H}^{S\,\mathrm{inc}} = \sum_g \left\{ \begin{matrix} \left(H_{gu}^{S\,\mathrm{inc}}\hat{\mathbf{u}} + H_{gv}^{S\,\mathrm{inc}}\hat{\mathbf{v}}\right) \\ \times \mathrm{e}^{-ik_{gx}\frac{1}{2}[z(w)+z^*(w^*)]+(k+g)\frac{1}{2}[z(w)-z^*(w^*)]+ik_s s} \end{matrix} \right\},$$
$$\mathbf{E}^{P\,\mathrm{inc}} = \sum_g \left\{ \begin{matrix} \left(E_{gu}^{P\,\mathrm{inc}}\hat{\mathbf{u}} + E_{gv}^{P\,\mathrm{inc}}\hat{\mathbf{v}}\right) \\ \times \mathrm{e}^{-ik_{gx}\frac{1}{2}[z(w)+z^*(w^*)]+(k+g)\frac{1}{2}[z(w)-z^*(w^*)]+ik_s s} \end{matrix} \right\}. \tag{11}$$

Once we know the transformation $z(w)$ these expressions can be expanded as waves in the w frame. The expansion typically converges accurately using terms of the order of 10–15 leading to computational efficiency. Reflected and transmitted waves can be expressed in a similar fashion.

These waves are now ready to be matched at the interface. In addition we must calculate the corresponding electric fields for the S polarized fields and magnetic fields for the P polarized case. In general there are two components parallel to the surface. The component along the s axis is calculated from Maxwell's equations in the metasurface frame then transformed into the slab frame; the component along the v axis is calculated from Maxwell's equations applied in the slab frame.

Matching the waves at the flat interface in the slab frame gives rise to a set of matrix equations that can be solved for the reflection and transmission coefficients. Details are straightforward but lengthy and are given in the Supplemental Material [26].

III. FIRST EXAMPLE

To show the effect of taking retardation into account we use a simple example provided by the transformation,

$$z = \Gamma \ln z' = \ln \frac{1}{w' - iw'_0} = \ln \frac{1}{e^w - iw'_0}. \tag{12}$$

This transformation gives rise to a rich sequence of metasurfaces [27].

For purposes of illustration we assume that the grating is made from a metal with permittivity of the Drude form,

$$\varepsilon(\omega) = 1 - \frac{\omega_p^2}{\omega(\omega + i\gamma)}. \tag{13}$$

We assume $\omega_p = 8$ eV, typical of a noble metal. The parameter γ represents resistive losses and is typically of the order of $0.1 - 0.2$ eV for the noble metals. However, for purposes of clarity when presenting dispersion curves we set γ to a very small value. If desired any functional form can be used for $\varepsilon(\omega)$.

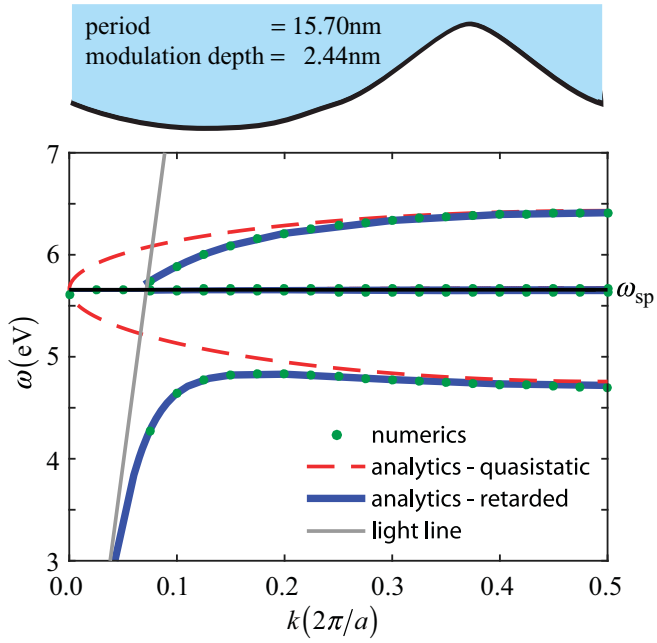

FIG. 3. Compares analytic theory with numerics of COMSOL calculations (shown as dots) for a metasurface pictured at the top of the figure. The analytic theory is essentially exact. Also shown are the light line and the quasistatic approximation as a dashed line.

Outside the metal we assume a vacuum. Other parameters are set to represent a relatively weak grating, approximately sinusoidal in form with a period, a, which is set to much less than the free space wavelength enabling coupling to surface plasmons:

$$\mathrm{w}_0 = 1.5, \quad \Gamma = 2.5\,\mathrm{nm}, \quad \mathrm{u}_0 = 1.0, \tag{14}$$

which implies a period of 15.7 nm and a modulation depth of 2.44 nm. See the Supplemental Material for a definition of u_0. Dispersion curves for wave vectors lying along the y axis are shown in Fig. 3. These were deduced from the reflection coefficients that show a peak due to coupling to surface plasmons when the dispersion relation is satisfied.

Note that the analytic theory is essentially exact with no divergence from COMSOL numerics. The dashed line shows the quasistatic theory that neglects retardation. As we have noted in earlier publications [27] the quasistatic solution reduces to the flat surface result at the zone center. The theory shows a plasmon polariton tracking the light line at low frequencies then hybridizing with the quasistatic result spoiling the degeneracy at the zone center. Near the zone boundary the quasistatic approximation is quite accurate revealing the dominant electrostatic nature of short wavelength solutions. In addition there is a multitude of shorter wavelength surface plasmon bands almost degenerate at the surface plasmon frequency. The grating being predominantly sinusoidal hardly splits these bands apart. More strongly modulated gratings do

give rise to splittings of these higher order bands but only at the zone boundary.

Between the light line and the zone center modes are not exact eigenstates but form resonances subject to radiative decay. However, coupling is primarily magnetic in nature: in the slab frame the transformed μ_s acquires a grating-like structure and couples surface plasmons to external radiation. Thus, the lower order modes are not well defined to the left of the light line as they dissolve into the continuum. However, since the higher order surface plasmons are primarily electrostatic in character, coupling is weak and radiative lifetimes are long and these modes are relatively well defined beyond the light line. We plot the trajectories of these resonance in Fig. 3.

The higher order modes hardly interact with this relatively weak grating and exhibit the near zero dispersion of the modes of a flat surface. This is a relatively trivial instance of slow light, which has been thoroughly discussed in Ref. [28].

At the Brillouin zone boundary a large band gap opens. Note that, typical of photonic systems, the lower state is depressed more that the upper state is raised. This has consequences for the zero point energy of the system: it would appear that at least as far as the dispersion relations are concerned a distortion of the surface is energetically favored. Of course there are other forces acting against an instability but significantly very many metal surfaces do show reconstructions of a grating-like form.

IV. SECOND EXAMPLE

One of the advantages of calculating reflection and transmission matrices is that further interfaces can be taken into account via multiple scattering theory. If a sample has two interfaces with transmission and reflection coefficients as defined in Fig. 4, then the combined system has reflection and transmission matrices as follows:

$$\begin{aligned} R^- &= r_1^- + t_1^+(1 - r_2^- r_1^+)^{-1} r_2^- t_1^-, \\ R^+ &= r_2^+ + t_1^+(1 - r_1^+ r_2^-)^{-1} r_1^+ t_2^+, \\ T^- &= t_2^-(1 - r_1^+ r_2^-)^{-1} t_1^-, \\ T^+ &= t_1^+(1 - r_2^- r_1^+)^{-1} t_2^+. \end{aligned} \tag{15}$$

In this way we calculate the reflectivity of a thin slab of metal one side of which is a planar interface with the vacuum, the other side a metasurface as defined above.

Figure 5 shows a check against simulations on the accuracy of our codes. The parameters used were as follows:

$$\mathrm{w}_0 = 0.8781, \quad \Gamma = 2.5\,\mathrm{nm}, \quad \mathrm{u}_0 = 0.8044. \quad d = 0.5, \tag{16}$$

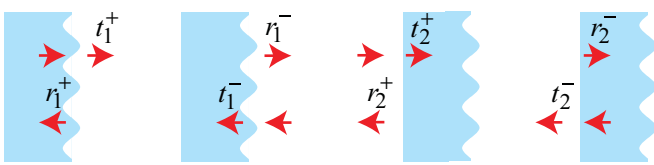

FIG. 4. Definition of the reflection and transmission coefficients at each surface of a grating of finite thickness.

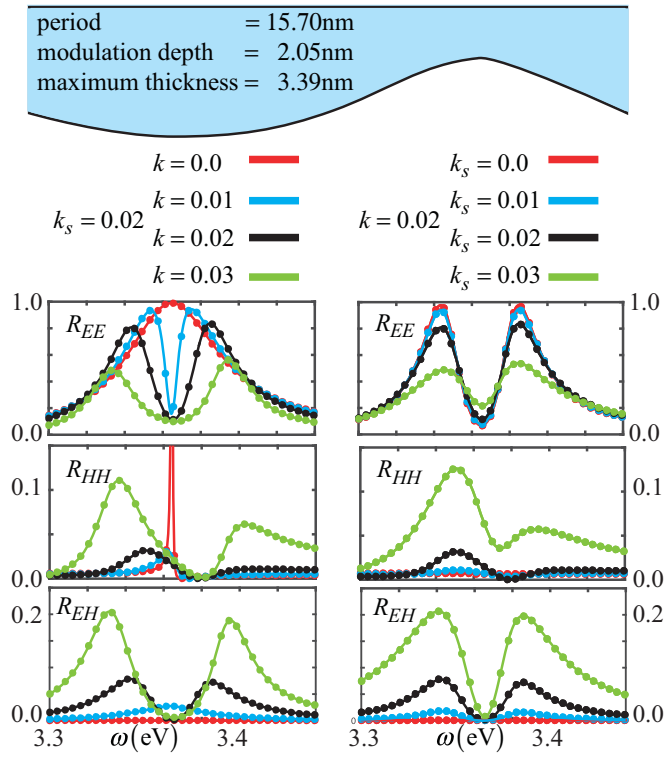

FIG. 5. Profile of the metasurface to scale followed by the total reflected intensity calculated as a function of frequency for various incident waves defined by k, k_s. Dots represent COMSOL calculations.

which implies a period of 15.7 nm and a modulation depth of 2.05 nm, and a maximum thickness of 3.39 nm. See the Supplemental Material for a definition of u_0 and d.

Hybrid modes form between the two surfaces that are approximately symmetric and antisymmetric. The thinner the grating the lower in frequency is the antisymmetric mode and we shall concentrate on this mode.

We identify modes by calculating reflection coefficients for various angles of incidence. Peaks in reflection identify frequencies of modes that are not perfectly defined because decay into the vacuum ensures a finite lifetime reflected in the finite widths of the peaks. Figure 5 plots reflectivities as a function of the wave vector parallel to the surface for two different directions.

The left column shows the reflectivity spectrum for a wave with incident wave vector contained in the $x - s$ plane ($k_s = 0.02$, $k = 0$, red line), as the incidence wave vector moves out of that plane, (k changing from 0.01 to 0.03, orange to green lines). The right column shows the corresponding results for nonzero k, as the plane of incidence goes out from the $y - x$ plane. While the upper and middle panel present the copolarized reflectivity for each polarization (R_{EE}, R_{HH}), the lower panel shows how the cross-polarized response (R_{EH}) becomes nonzero when the plane of incidence does not correspond with the symmetry planes of the metasurface.

Extracting the band dispersion from these figures yields Fig. 6. In this instance the modes are well defined to the left of the light line and form well-defined sharp resonances enabling us to continue the dispersion relationship into this region. This is because their subwavelength nature inhibits coupling to the

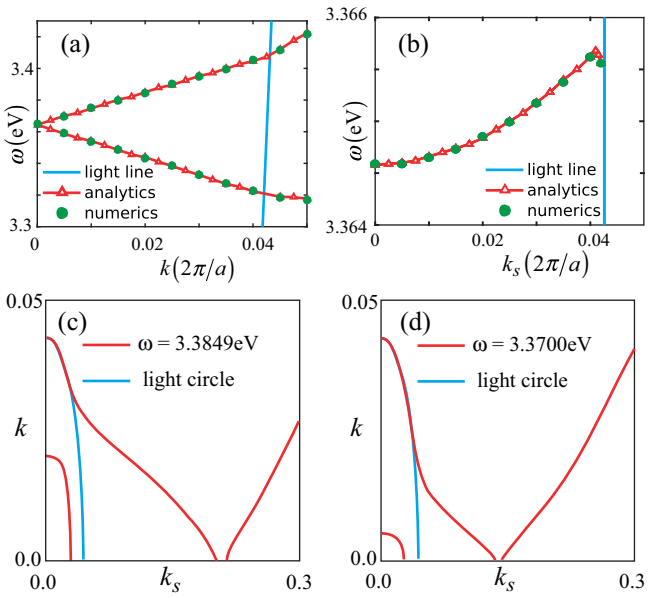

FIG. 6. Dispersion of surface plasmon modes for two polarizations as defined in the supplemental material (a) S polarized and (b) P polarized. Note the differing frequency scales. Dots represent COMSOL calculations. (c) and (d) show intersections of dispersion surfaces for the same grating. Note the strong dispersion with k and weak dispersion with k_s requiring different scales for each, hence distorting circles into ellipses. Except for the intrusion of the light circle, the curves approximately represent two circles intersecting near $k = 0,\ k_s = 0.2$.

far field. Note the degeneracy at the zone center in Figs. 6(a) and 6(b) which is exact in the quasistatic limit, the linear dispersion with k, and the quadratic dispersion with k_s. In the latter case the single band shown is in fact doubly degenerate at the origin and approximately so at other values of k_s, though the splitting is too small to show in this scale. Again note the perfect agreement with the numerics.

Another way to display dispersion is to present sections of the isofrequency surfaces; two of which are given in Figs. 6(c) and 6(d). Note the different scales on the two axes distorting the light circle into an ellipse. In the limit of a weak grating and the quasistatic approximation, dispersion is represented by two intersecting cones appearing as intersecting circles in an isofrequency plot. However when retardation is brought into play the light circle and surface plasmons hybridize and a gap opens at the intersection of the cones. All states within the light cone have finite radiative lifetimes.

V. CONCLUSIONS

We have demonstrated a methodology for making accurate quasianalytic calculations for an arbitrary 1D metasurface. The theory has been tested against COMSOL simulations. The theory is based on conformal mapping interpreted though transformation optics theory, linking the theory to many approximate results obtained in the quasistatic approximation. Our analytic calculations are typically one or two orders of magnitude faster than the numerical codes. Detailed derivations for the two examples given above are presented in the Supplemental Material.

ACKNOWLEDGMENTS

J.B.P. and K.D. acknowledge support from the Gordon and Betty Moore Foundation. P.A.H. acknowledges funding from a Marie Sklodowska-Curie Fellowship and the Gordon and Betty Moore Foundation.

[1] A. J. Ward and J. B. Pendry, J. Mod. Opt. **43**, 773 (1996).
[2] J. B. Pendry, D. Schurig, and D. R. Smith, Science **312**, 1780 (2006).
[3] U. Leonhardt, Science **312**, 1777 (2006).
[4] D. Schurig, J. J. Mock, B. J. Justice, S. A. Cummer, J. B. Pendry, A. F. Starr, and D. R. Smith, Science **314**, 977 (2006).
[5] H. Y. Chen, C. T. Chan, and P. Sheng, Nat. Mater. **9**, 387 (2010).
[6] J. H. Jeans, *The Mathematical Theory of Electricity and Magnetism* (Cambridge University Press, Cambridge, 1911).
[7] Y. Liu, T. Zentgraf, G. Bartal, and X. Zhang, Nano Lett. **10**, 1991 (2010).
[8] J. B. Pendry, A. Aubry, D. R. Smith, and S. A. Maier, Science **337**, 549 (2012).
[9] J. B. Pendry, Yu. Luo, and R. Zhao, Science **348**, 521 (2015).
[10] R.-Q. Li, D. Hernángomez-Pérez, F. J. García-Vidal, and A. I. Fernández-Domínguez, Phys. Rev. Lett. **117**, 107401 (2016).
[11] E. Popov (ed.), *Gratings: Theory and Numeric Applications, Second Revisited Edition* (2014), http://www.fresnel.fr/files/gratings/Second-Edition.
[12] J. Chandezon, D. Maystre, and G. Raoult, J. Opt. **11**, 235 (1980).
[13] W. L. Barnes, T. W. Preist, S. C. Kitson, and J. R. Sambles, Phys. Rev. B **54**, 6227 (1996).
[14] A. V. Kildishev, A. Boltasseva, and V. M. Shalaev, Science **339**, 1289 (2013).
[15] N. Yu, P. Genevet, M. A. Kats, F. Aieta, J.-P. Tetienne, F. Capasso, and Z. Gaburro, Science **334**, 333 (2011).
[16] N. Yu and F. Capasso, Nat. Mater. **13**, 139 (2014).
[17] N. Meinzer, W. L. Barnes, and I. R. Hooper, Nat. Photon. **8**, 889 (2014).
[18] A. E. Minovich, A. E. Miroshnichenko, A. Y. Bykov, T. V. Murzina, D. N. Neshev, and Y. S. Kivshar, Laser Photon. Rev. **9**, 195 (2015).
[19] S. B. Glybovski, S. A. Tretyakov, P. A. Belov, Y. S. Kivshar, and C. R. Simovski, Phys. Rep. **634**, 1 (2016).
[20] F. Monticone and A. Alù, Rep. Prog. Phys. **80**, 036401 (2017).
[21] S. A. Maier, *Plasmonics: Fundamentals and Applications* (Springer, Boston, MA, 2007).

[22] J. B. Pendry, P. A. Huidobro, Yu. Luo, and E. Galiffi, Science **358**, 915 (2017).

[23] M. J. Ablowitz and A. S. Fokas, *Complex Variables: Introduction and Applications* (Cambridge University Press, Cambridge, 2003).

[24] P. A. Huidobro, Y. H. Chang, M. Kraft, and J. B. Pendry, Phys. Rev. B **95**, 155401 (2017).

[25] N. B. Kundtz, D. R. Smith, and J. B. Pendry, Proc. IEEE **99**, 1622 (2011).

[26] See Supplemental Material at http://link.aps.org/supplemental/10.1103/PhysRevB.99.085408 for details of programing.

[27] M. Kraft, Yu. Luo, S. A. Maier, and J. B. Pendry, Phys. Rev. X **5**, 031029 (2015).

[28] K. L. Tsakmakidis, O. Hess, R. W. Boyd, and X. Zhang, Science **358**, 319 (2017).